Advanced Robotics, Vol. 17, No. 4, pp. 319–337 (2003)

Also available online - www.vsppub.com

Full paper

Automatic concrete tunnel inspection robot system

FENGHUI YAO [1,*], GUIFENG SHAO [2], RYOICHI TAKAUE [1] and AKIKAZU TAMAKI [1]

[1] *University of East Asia, 2-1 Ichinomiyagakuen–machi, Shimonoseki, 751-8503, Japan*
[2] *Seinan Gakuin University, 6-2-92 Nishijin, Sawara-ku, Fukuoka, 814-0002, Japan*

Received 15 March 2002; accepted 14 June 2002

Abstract—This paper describes the development of an automatic concrete tunnel inspection system by an autonomous mobile robot. This work was motivated by the accidents in recent years that were caused by falling parts of the inner wall of concrete tunnels. This brought about serious damage to national property and led to the great concern throughout the whole society. Here, we proposed a non-destructive automatic tunnel inspection method. In this method, we aim to inspect the tunnel automatically and completely at high speed by using non-destructive sensors. For the non-destructive sensors, we employ 24 ultrasonic range sensors and six video cameras. These sensors are mounted on the same plane in the shape of a semi-ring. This ultrasonic range sensor video camera semi-ring is called a URS/VC semi-ring. This URS/VC semi-ring is mounted on an autonomous mobile robot to inspect the concrete tunnel. Experiment results show that this system can detect deformed inner walls at divisions of 14 mm when the robot moves at 20 mm/s.

Keywords: Autonomous mobile robot; oncrete tunnel inspection; URS/VC semi-ring; inspection robot system; extended EERUF algorithm.

1. INTRODUCTION

In Japan, many concrete tunnels have been constructed on railways, highways and roads in the last 30 years, and this construction seems to be on-going. However, many accidents have happened recently that were caused by falling parts of the inner wall of concrete tunnels. In the following, the concrete tunnel is simply shorted as 'tunnel'. The tunnel accidents brought about serious damage to national property and led to the great concern throughout the whole society. These accidents may happen become more frequent from now on because it is more than 30 years since some of the tunnels were constructed. To avoid these accidents, it is necessary to

*To whom correspondence should be addressed. Present address: 3-14-40501 Agenogi, Matsue-shi, Shimane-ken 690-0015, Japan. E-mail: yao@ipc.shiman-u.ac.jp

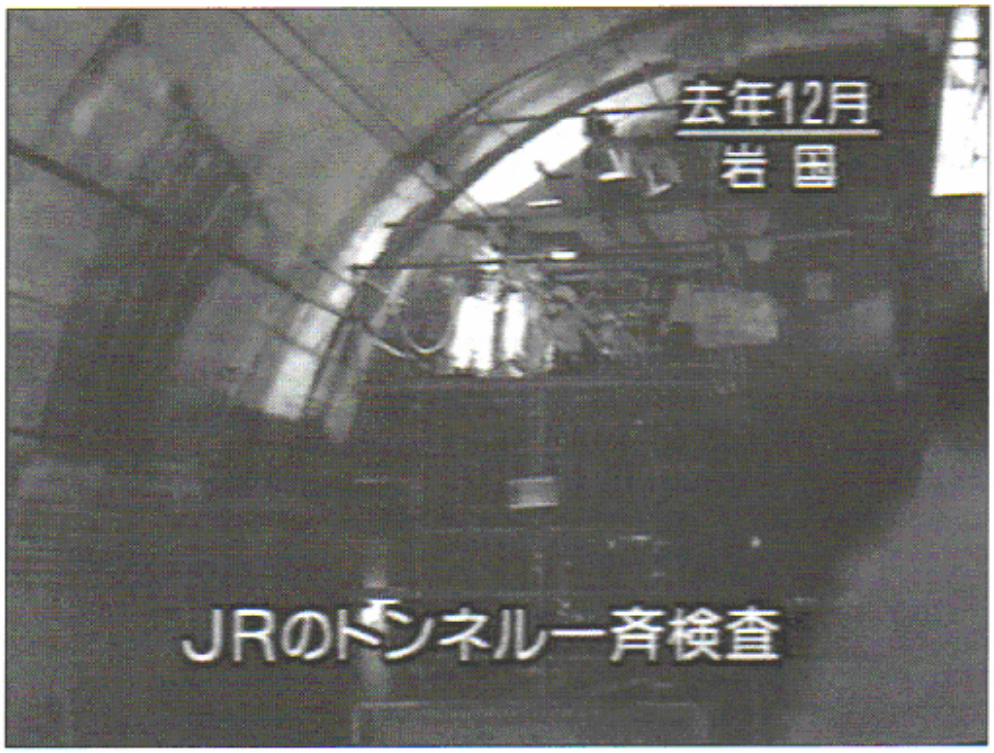

Figure 1. Traditional concrete tunnel inspection scene (photo courtesy of KRY).

inspect the tunnels periodically and detect the particular parts of the inner wall of the tunnel that may fall down in the near future. The traditional inspection method is the that of 'hammer-knocking'. Figure 1 shows one inspection scene of this method, in which people stand on a movable platform and knock the inner wall of the tunnel with a hammer and then determine whether the knocked area is normal or not according to the echo. This traditional method has the following disadvantages: (i) the evaluation is subjective and there is the problem of reliability; (ii) it is difficult to knock the whole tunnel and there exists areas which are not be inspected; (iii) it will take tremendous labor and a long time to inspect all tunnels completely; and (iv) the knocks on the inner wall, from the long–term point of view, will damage the tunnel.

Here, we propose a non-destructive automatic tunnel inspection method [1]. In this method, we aim to inspect the tunnel automatically and completely at high speed by employing non-destructive sensors. Among non-destructive sensors, the ultrasonic sensor is cheap and reliable, and has been widely used in indoor mobile robot navigation and obstacle avoidance [2–6]. However, the ultrasonic sensor can only detect the existence of objects and one ultrasonic sensor can only output one point data. It cannot give any further information about objects. Therefore, we propose to use the fusion of visual and plural ultrasonic sensors to inspect the tunnel inner wall. In our prototype system, we employ 24 ultrasonic range sensors and six video cameras. These ultrasonic range sensors and video cameras are mounted in a semi-ring. This ultrasonic range sensor video camera semi-ring is called the

URS/VC semi-ring in the following. The purpose of the URS semi-ring is to detect shape deformation of the tunnel, e.g. 'swell' or 'hollow', and the purpose of the VC semi-ring is to detect structural or surface changes, e.g. 'cracking' and 'water penetration status through the crack'. The combination of the URS semi-ring and VC semi-ring can allow precise inspection. At present, only the URS semi-ring is ultilized. The VC semi-ring is under development. Therefore, this paper focuses on tunnel deformation detection. The combination with the VC semi-ring will be described in another paper. The remainder of this paper is organized as follows. Section 2 describes the design of the URS/VC semi-ring. Section 3 presents the algorithm to fire the URS semi-ring. Section 4 shows the principles of automatic tunnel inspection. Section 5 gives the experimental results. The paper finishes with conclusions and remarks.

2. DESIGN OF THE URS/VC SEMI-RING

The left-hand Cartesian coordinate system is employed in the configuration of the URS/VC semi-ring, where $+Y$ points to the front, $+X$ the left and $+Z$ upward. This is the same as with autonomous mobile robots. For implementation convenience, each ultrasonic sensor and video camera in the URS/VC semi-ring has a different radius as shown in Fig. 2. Let S_j represent the jth ultrasonic sensor, R_j express the radius from S_j to the origin of the URS/VC semi-ring and ϕ_j denote the angle from $+X$ to S_j. Let V_k represent the kth video camera, L_j express the radius from V_k to the origin of the URS/VC semi-ring and ψ_k denote the angle from $+X$ to V_k. Their values are given in Table 1.

The Polaroid 600 series is chosen as URS elements [7]. A comprehensive discussion of the characteristics and limitations of these sensor elements can be found in the literature [3, 8, 9]. In order to guarantee complete coverage of the area over the URS semi-ring, 24 URSs were installed at 7.5° intervals (except those intervals between S_0 and S_1, S_1 and S_2, S_{21} and S_{22}, S_{22} and S_{23}). Kuc shows that theoretically it would be necessary to use even denser spacing (e.g. 5°) to cover all possible obstacles [10]. However, Borenstein and Koren found that in practice 15° spacing reliability detected obstacles as small as 8-mm diameter vertical poles [2]. Similar designs using 24 URSs in 15° intervals are described in the literature [11, 12].

This URS/VC semi-ring is settled on an autonomous mobile robot. The mobile robot also employs the left-hand Cartesian coordinate system. The origin is located at the center of the mobile robot in the X- and Y-axes, and 291 mm high from the ground for Z-axis. The whole autonomous mobile robot system mounted with the URS/VC semi-ring is shown in Fig. 3.

At present, only ultrasonic sensors are mounted on the URS/VC semi-ring and we employed this URS/VC semi-ring to detect deformations of the tunnel inner wall, e.g. convex and concave. Convex means that the corresponding part of the tunnel

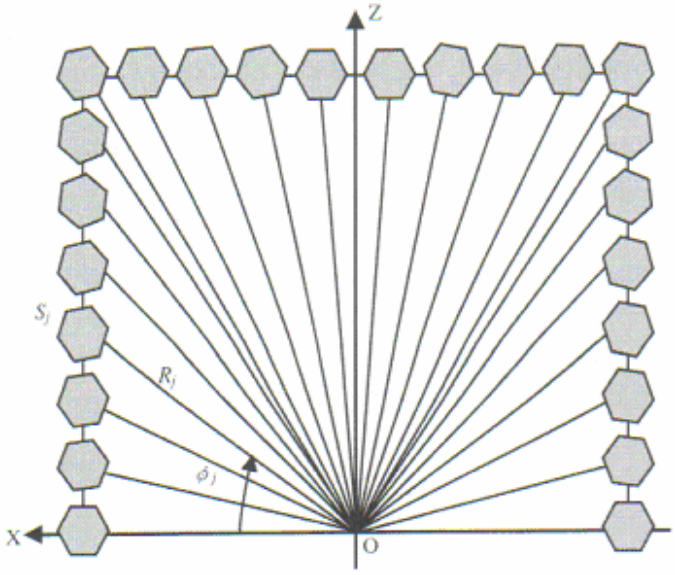

Figure 2. Cofiguration of the URS/VC semi-ring.

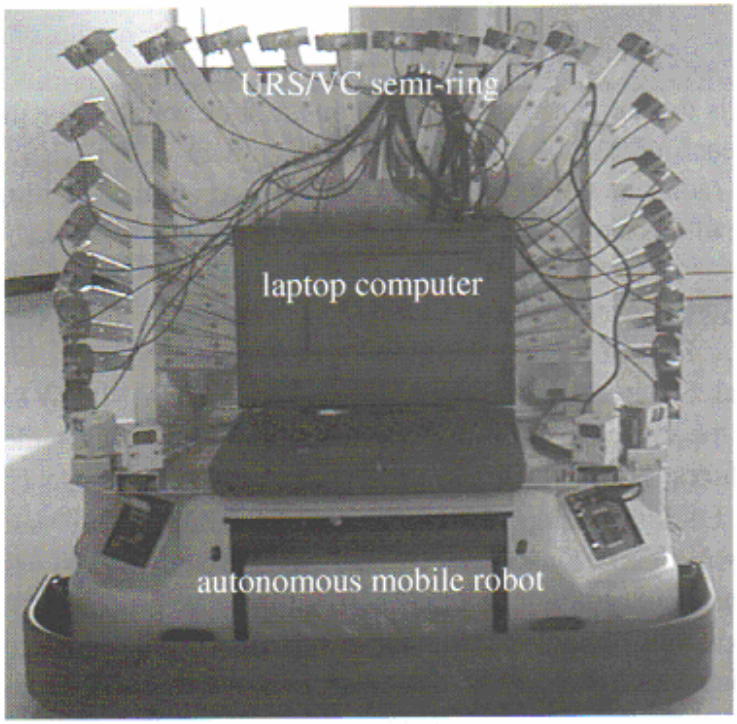

Figure 3. An autonomous mobile robot mounted with the URS/VC semi-ring.

inner wall has a large probability of falling down in the near future and concave means that the corresponding part has already fallen.

3. ALGORITHM TO FIRE THE URS SEMI-RING

As pointed by Borenstein and Koren [1], using multiple URSs increases the amount of ultrasonic noise in the environment in two ways: (i) environmental noise from

Table 1.
Angles and radii of ultrasonic sensors and video cameras in the URS/VC semi-ring

S_j/C_k	ϕ_j (deg)	R_j (cm)	ψ_k (deg)	L_k (cm)
0	0	34.5		
1	5.2	34.5		
2	14.5	34.5		
3/0	26	37.7	26	37.7
4	33.5	40.1		
5	41	43.6		
6/1	48.5	48.8	48.5	48.8
7	56	54.7		
8	63.5	51.2		
9/2	71	48.8	71	48.8
10	78.5	47.3		
11	86	46.6		
12	94	46.6		
13	101.5	47.3		
14/3	109	48.8	109	48.8
15	116.5	51.2		
16	124	54.7		
17/4	131.5	48.8	131.5	48.8
18	139	43.6		
19	146.5	40.1		
20/5	154	37.7	154	37.7
21	165.5	34.5		
22	174.8	34.5		
23	180	34.5		

other ultrasonic sensors and (ii) internal noise from onboard ultrasonic sensors — crosstalk. These two issues also exist in this tunnel inspection robot system. Type (i) noise is typically a discrete disturbance. It is likely to occur when more than one robot with ultrasonic sensors operates in the same environment. In this case, interference may occur over distances of up to 20 m. Crosstalk (also called multipath) is an undesirable phenomenon in which one sensor receives the ultrasonic waves emitted by another sensor. Figure 4 shows an inspection mobile robot equipped with multiple URSs in two situations in a tunnel environment. Both situations differ substantially in the way they promote crosstalk. For the following discussion, the term 'critical path' is employed, which is defined as any path of ultrasound waves that are transmitted by one sensor and are received by one or more others. The sensor that transmitted the ultrasound waves is labeled S_m and each of the receiving sensors is labeled S_n. Figure 4a shows a direct critical path, where sensors S_n are on a critical path with sensor S_m. If any sensor S_n fired shortly after sensor S_m, this sensor S_n would be awaiting the echo to its own signal by the time the echo from sensor S_m reaches it. Thus, the reading from sensor S_n would result in some arbitrary error, depending on the time difference, T_{lag}, between firing

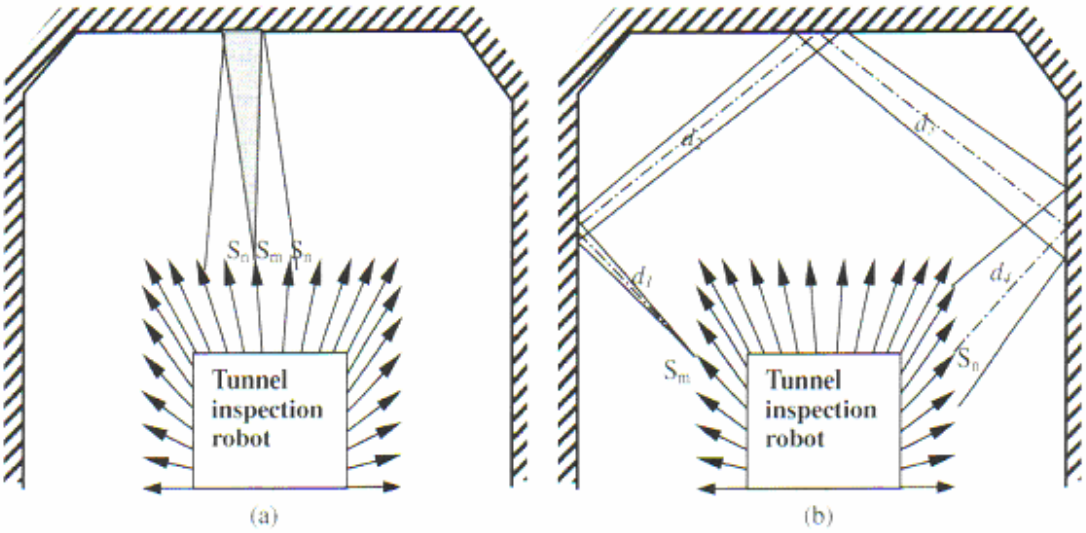

Figure 4. How crosstalk from onboard sensors is generated. (a) Direct critical path. (b) Indirect critical path.

sensors S_m and S_n. Figure 4b shows the indirect critical path. Here, at an instance t_0, sensor S_m fires and its ultrasound waves are reflected off three inner walls of the tunnel. Assuming the walls are fairly smooth, the reflected wavefront will reach sensor S_n after traveling through the distance $D = d_1 + d_2 + d_3 + d_4$. If, at this time, the sensor S_n is awaiting an echo of its own, then it will receive the signal from sensor S_m and interpret it as its own echo. These two critical paths can be easily satisfied in the tunnel environment.

In order to reject interference and crosstalk, several works have been done [2, 13, 14]. Here, we extend the Error Eliminating Rapid Ultrasonic Firing (EERUF) algorithm to fire the URS semi-ring. The EERUF algorithm was designed by Borenstein and Koren for mobile robot obstacle avoidance with 12 ultrasonic sensors [1]. The EERUF algorithm works as follows. To overcome non-systematic external noise and systematic error caused by crosstalk, the delay (T_{wait}) is alternated before each sensor fires. For each sensor S_i, T_{wait} alternates between two values, a_i and b_i. a_i and b_i can be very small, of the order of a few milliseconds. Now, any sensor S_i can re-fire immediately after receiving the echo and after waiting for the short delay, $T_{\text{i,wait}}$. After each firing, $T_{\text{i,wait}}$ is toggled between $T_{\text{i,wait,a}}$ and $T_{\text{i,wait,b}}$. We extended this EERUF algorithm to the URS semi-ring that consists of 24 ultrasonic sensors. The modified firing schedule is shown in Table 2. The theoretical analysis is given in the literature [2]. Details are omitted here. In Table 2, T_{lag} is the amount of time that a sensor is scheduled for firing after the beginning of a period; T_{wait} is the amount of time that EERUF waits before firing a sensor, after the sensor was already scheduled for firing; T_{fire} is the amount of time from the beginning of a period to the actual firing of a sensor.

Table 2.
Modified firing schedule for ultrasonic sensors in the URS semi-ring

S_i	T_{lag} (ms)	$T_{wait,a}$ (ms)	$T_{wait,b}$ (ms)	$T_{fire,a}$ (ms)	$T_{fire,b}$ (ms)
0	0	24	42	24	42
1	25	24	36	49	61
2	50	24	30	74	80
3	75	24	24	99	99
4	100	24	18	124	118
5	125	24	12	149	137
6	150	24	6	174	156
7	175	24	0	194	175
8	0	24	44	24	44
9	25	24	38	49	63
10	50	24	32	74	82
11	75	24	26	99	101
12	100	24	20	124	120
13	125	24	14	149	139
14	150	24	8	174	158
15	175	24	2	194	177
16	0	24	46	24	46
17	25	24	40	49	65
18	50	24	34	74	84
19	75	24	28	99	103
20	100	24	22	124	122
21	125	24	16	149	141
22	150	24	10	174	160
23	175	24	4	194	179

4. AUTOMATIC TUNNEL INSPECTION PRINCIPLE

Our method of automatic tunnel inspection consists of two steps. The first step is the construction of the standard tunnel model. The standard tunnel model means the model of the tunnel without deformation. The standard tunnel model is constructed in advance by running the autonomous mobile robot through the whole tunnel. The second step is the automatic tunnel inspection. This is performed periodically, e.g. once a month. Our principle is to perform automatic tunnel inspection continuously while the autonomous mobile is moving. The inspection system detects the shape of the tunnel inner wall and constructs the tunnel model. Then it performs partial matching between the standard tunnel model and the newly constructed tunnel model (the update tunnel model). If the matching error exceeds the predetermined threshold value, the system will make a mark (e.g. a red point) at the place where the deformation exists.

The following presents the details of the tunnel model construction and tunnel model matching.

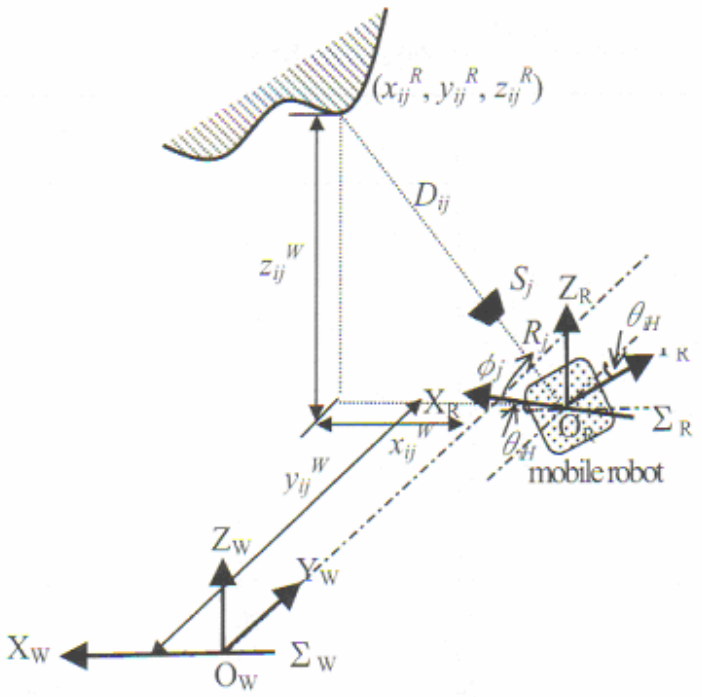

Figure 5. Sensor reading and coordinates in Σ_R and Σ_W.

4.1. Tunnel model construction

Let Σ_W express the world coordinates system, and $(x_{ij}^W, y_{ij}^W, z_{ij}^W)$ a point obtained from the reading of S_j at time t_i in Σ_W. The place where the system is powered on is the origin of Σ_W. Let $(x_{iR}, y_{iR}, \theta_{iH})$ represent the x, y position and the heading of the mobile robot at time t_i in Σ_W. Further, let Σ_R represent the mobile robot coordinate system and $(x_{ij}^R, y_{ij}^R, z_{ij}^R)$ a point obtained from the reading of S_j at time t_i in Σ_R. Because Σ_R moves together with the mobile robot, it is called the relative robot coordinate system. For the range data D_{ij} from the sensor S_j $(j = 0, 1, \ldots, 23)$ at time t_i, it is converted to the coordinates in Σ_R according to (1)–(3) as shown in Fig. 5:

$$x_{ij}^R = (D_{ij} + R_j)\cos\phi_j, \tag{1}$$

$$y_{ij}^R = 0, \tag{2}$$

$$z_{ij}^R = (D_{ij} + R_j)\sin\phi_j, \tag{3}$$

where ϕ_j is the angle from the $+x$-axis and R_j is the radius of sensor S_j.

Figure 5 shows the origin of Σ_W, and the position and orientation of the mobile robot in Σ_W. Considering the heading of the mobile robot, the coordinates in (1)–(3) must be rotated before changing to the coordinates in Σ_W. In fact, the y-position of the mobile robot is just the y-coordinates of range data D_{ij} in Σ_W. As because the mobile robot is working on the XOY-plane of Σ_W, z-coordinate in (3) is the same as that in Σ_W. Therefore, only the x-coordinate in (1) needs

to be rotated. From these considerations, $(x_{ij}^{\mathrm{R}}, y_{ij}^{\mathrm{R}}, z_{ij}^{\mathrm{R}})$ is converted to the world coordinates as follows:

$$x_{ij}^{\mathrm{W}} = x_{ij}^{\mathrm{R}} \cos\phi_{i\mathrm{H}} - x_{i\mathrm{R}}, \tag{4}$$

$$y_{ij}^{\mathrm{W}} = y_{ij}^{\mathrm{R}} + y_{i\mathrm{R}}, \tag{5}$$

$$z_{ij}^{\mathrm{W}} = z_{ij}^{\mathrm{R}}. \tag{6}$$

All the readings from $S_0, \ldots, S_{23}$ are converted to the world coordinates while the autonomous mobile robot runs through the whole tunnel. The tunnel model is constructed from these world coordinates.

4.2. Matching

In the tunnel inner wall inspection, the ultrasonic sensors in the URS/VC semi-ring are fired repeatedly according to EERUF algorithm while the autonomous mobile robot moves through the whole tunnel. All readings from the sensors are converted to the world coordinates. With these coordinates data, we can construct the updated tunnel model. Let T_{S} and T_{U} represent the standard tunnel model and updated tunnel model, respectively. The matching between T_{S} and T_{U} is performed in the following procedures:

(i) T_{U} is translated so that its start point overlaps with that of T_{S}.

(ii) T_{U} is rotated so that its terminal point overlaps with that of T_{S}.

(iii) The matching error between the corresponding points in T_{S} and T_{U} is calculated. Here, we employ the Euclidean distance between the corresponding points in T_{S} and T_{U} as the matching error, i.e.:

$$E_{ij} = \left\| P_{ij}^{\mathrm{WS}} - P_{i'j}^{\mathrm{WU}} \right\|, \quad (i = 0, 1, \ldots, M,\ j = 0, 1, \ldots, 23), \tag{7}$$

where P_{ij}^{WS} and $P_{i'j}^{\mathrm{WU}}$ are the points in T_{S} and T_{U}, respectively, i.e. $P_{ij}^{\mathrm{WS}} = (x_{ij}^{\mathrm{WS}}, y_{ij}^{\mathrm{WS}}, z_{ij}^{\mathrm{WS}})$ and $P_{i'j}^{\mathrm{WU}} = (x_{i'j}^{\mathrm{WU}}, y_{i'j}^{\mathrm{WU}}, z_{i'j}^{\mathrm{WU}})$, and M is the data number read from the URS semi-ring.

It is worth to noting that although T_{U} is translated and rotated so that its starting point and terminal point overlap with those of T_{S}, the points on T_{S} and T_{U} at an instance t_i (from the beginning of the inspection) may not overlap because of the movement error of the mobile robot. Therefore, the point P_{ij}^{WS} on T_{S} should be mached with such a point $P_{i'j}^{\mathrm{WU}}$ (on T_{U}) that satisfies $\left\lfloor y_{i'j}^{\mathrm{WU}} \right\rfloor = y_{ij}^{\mathrm{WS}}$, when calculating the matching error according to (7). The size of the matching error map is $M \times 24$ bytes. The image processing techniques can be applied to it as follows.

(iv) The matching error E_{ij} obtained according to (7) is binarized into '1' and '0' with the predetermined threshold value E_{T}, where '1' means the matching error

is bigger than E_T. Let $\bar{E}_{ij}$ express the binarized matching error. The next is to label '1'-clumps in $\bar{E}_{ij}$ and let $C_0, \ldots, C_{N-1}$ represent the '1'-clumps in $\bar{E}_{ij}$. If the number of '1' is C_i $(i = 0, 1, \ldots, N-1)$ is smaller than the threshold value N_T, C_i is discarded. After this filtering operation, the remaining '1'-clumps correspond to the places of defromation in T_U, that are re-denoted by C_k $(k = 0, 1, \ldots, N'-1)$.

4.3. Deformation measurement

For the deformation C_k, its width and length can be represented by those of its circumscribed rectangle. The width W of C_k is calculated according to the (8) and (9) as show in Fig. 6:

$$W = \sum_{S_m} d_m, \tag{8}$$

$$d_m = \left(r_m^2 + r_{m+1}^2 - 2r_m r_{m+1}\cos\beta_m\right)^{1/2}, \tag{9}$$

where S_m means the sensor whose reading lies in C_k, r_m is the sum of the reading and radius of S_m, r_{m+1} is the sum of the reading and radius of S_{m+1} and $\beta_m = \phi_{m+1} - \phi_m$.

However, the width obtained from (8) is not the real size of C_k. It is larger than the real size. This is because the ultrasonic beam spreads. For example, the sensor S_k, as shown in Fig. 6, can also detect the deformation C_k. Therefore, (8) should be corrected as:

$$W = \sum_{S_m} d_m - 2d_R, \tag{10}$$

$$d_R \approx \left(\left(D_k \sin\frac{\alpha}{2}\right)^2 + \left(D_k - D_k\cos\frac{\alpha}{2}\right)^2\right)^{1/2} = D_k\left(2 - 2\cos\frac{\alpha}{2}\right)^{1/2}, \tag{11}$$

where D_k is the reading from S_K and α is the opening of the ultrasonic sensor.

Likewise, the length of C_k can be calculated by (refer to Fig. 7):

$$L = y_{vR} - y_{uR} - 2d_F, \tag{12}$$

$$d_F \approx \left(\left(D_{um} \sin\frac{\alpha}{2}\right)^2 + \left(D_{um} - D_{um}\cos\frac{\alpha}{2}\right)^2\right)^{1/2} = D_{um}\left(2 - 2\cos\frac{\alpha}{2}\right)^{1/2}, \tag{13}$$

where D_{um} is the reading of S_m at time t_u (the front edge of C_k), y_{uR} is the y-coordinates of the autonomous mobile robot at time t_u and y_{vR} at time t_v (the rear edge of C_k).

The height H_k of C_k is given by:

$$H_k = \frac{1}{N_{C_k}} \sum_{C_k} e_k, \tag{14}$$

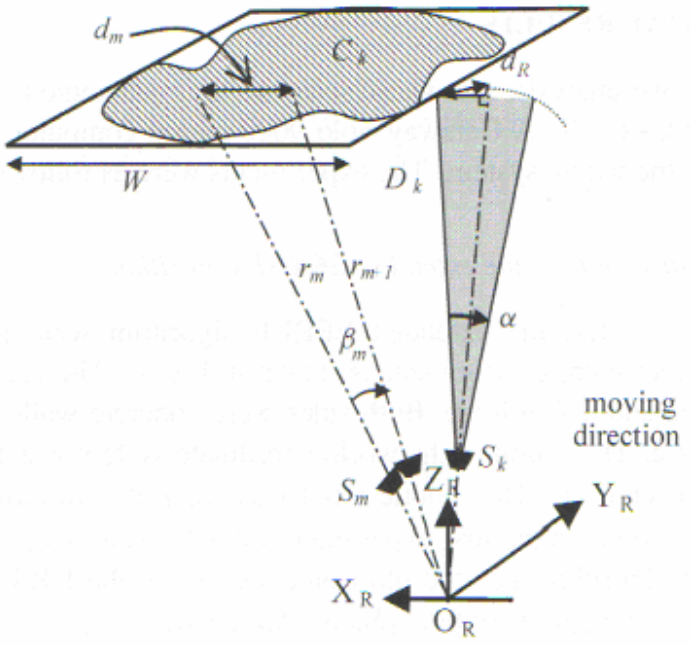

Figure 6. Width calculation of the deformation area.

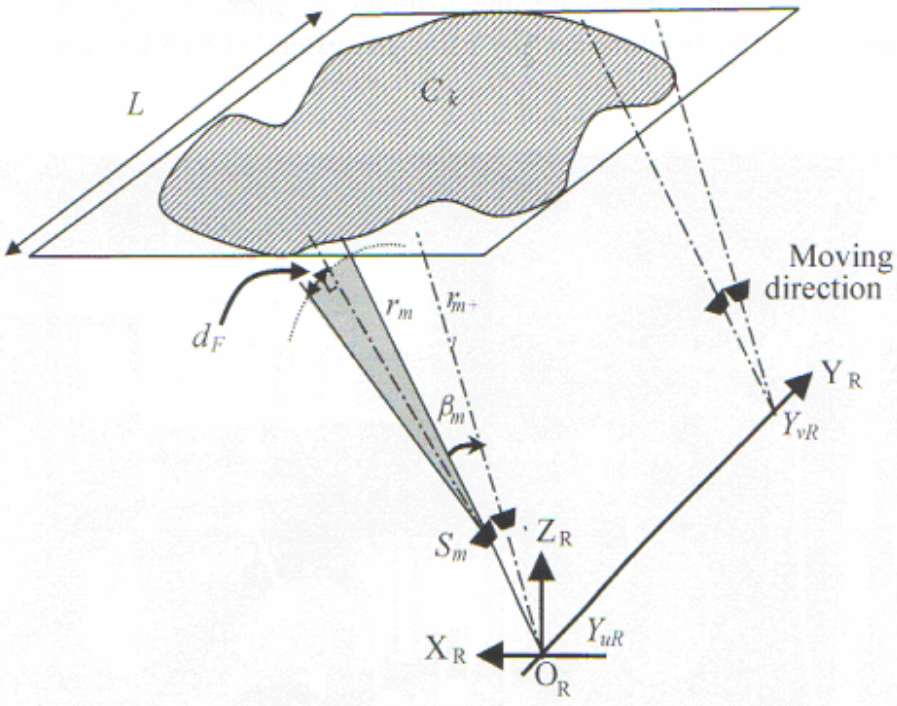

Figure 7. Length calculation of the deformation area.

where N_{C_k} is the total number of '1s' in C_k and e_k is the matching error of the points in C_k. H_k is the mean of the thickness of C_k and is used to calculate the volume of C_k. According to (8), (12) and (14), the area and volume of C_k can be obtained.

5. EXPERIMENTAL RESULTS

Based on the above analysis, the whole software is implemented on Windows 98 with MS-Visual C++ 6.0. A Gateway Solo 9000 laptop computer is employed as the controller of the whole system. The experiments were as follows.

5.1. Experimental results of the extended EERUF algorithm

The experiments to test the extended EERUF algorithm were performed in a corridor. The experiment environment is shown in Fig. 8. The corridor was 20 m long, 4.3 m wide and 2.7 m high. Both sides were concrete walls and the ceiling was a plaster plate. The origin of the world coordinate system was the point where the system is powered on. The mobile robot was controlled to move 2 m forward from the starting point. In the first experiment, the URS semi-ring was fired by the sequential firing algorithm, i.e. the ultrasonic sensors in the URS semi-ring were fired in the following group order: $\{S_0, S_8, S_{16}\}$, $\{S_1, S_9, S_{17}\}, \ldots, \{S_7, S_{15}, S_{23}\}$, where $\{.\}$ means to fire simultaneously. The sensors with heavy error readings are S_7, S_9, S_{10}, S_{15} and S_{16} as shown in Fig. 9. It contains both interferences and crosstalks. The same experiment was repeated by using the extended EERUF algorithm. The readings from the same channels are shown in Fig. 10. It is clear that the error reading is eliminated by using the extended EERUF algorithm (see Section 3).

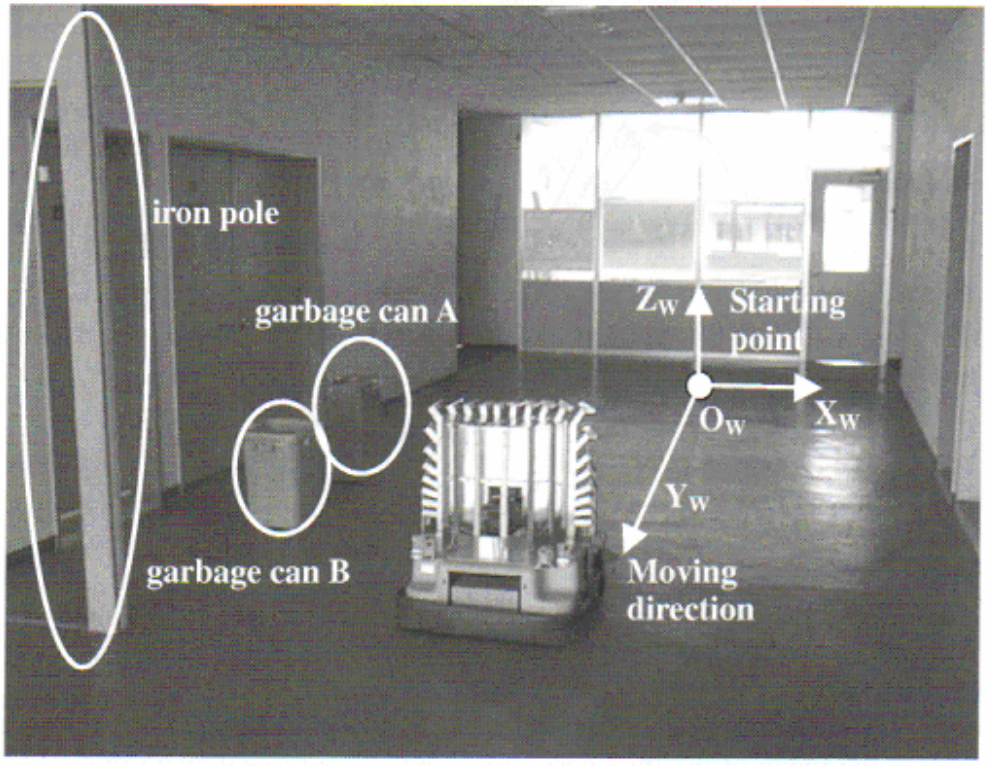

Figure 8. Experiment environment.

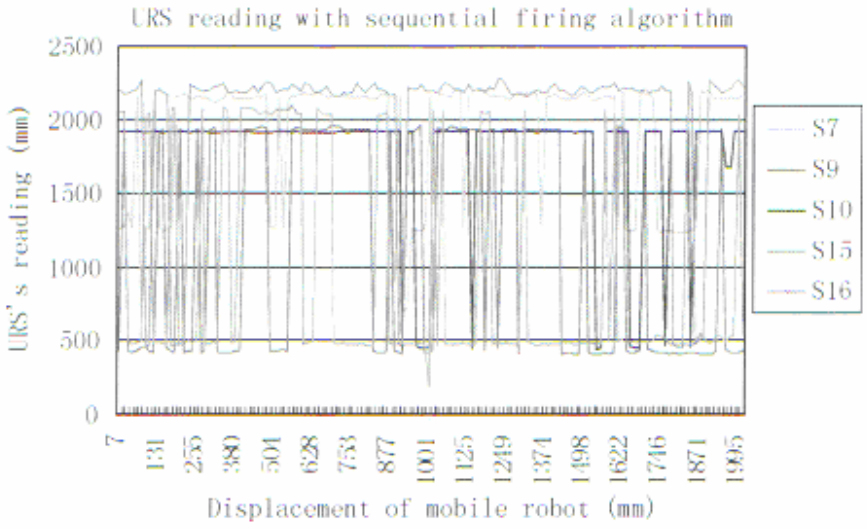

Figure 9. Readings from S_7, S_9, S_{10}, S_{15} and S_{16} with the sequential firing algorithm.

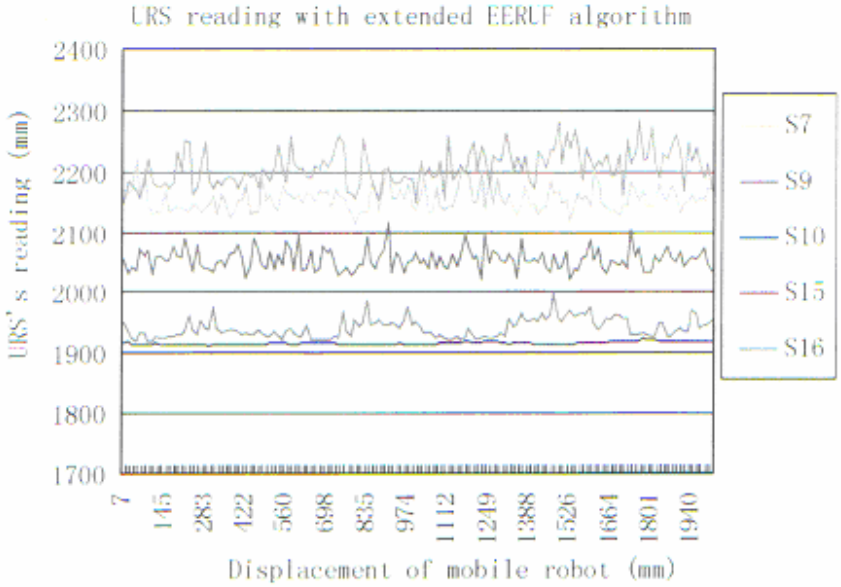

Figure 10. Readings from S_7, S_9, S_{10}, S_{15} and S_{16} with the extended EERUF algorithm.

5.2. Tunnel model construction experiment results

This experiment was performed to show how precise the tunnel model can be constructed. The experiment environment was the same as in the previous experiment as shown in Fig. 8. The speed of the mobile robot was set at 20 mm/s. Part of the constructed corridor model is shown in Fig. 11 as a wireframe model. Figure 11a–c shows the left side wall, the ceiling and the right side wall of the corridor, respectively. All are well constructed. The moving distance interval between two successive read-commands from the controller of the system is 14 mm. That is, the division of this inspection robot is 14 mm when it moves at 20 mm/s. It is worth to noting that the outputs of all sensors in the URS semi-ring will be read by one read-command sending to the URS semi-ring. The constructed corridor model of a

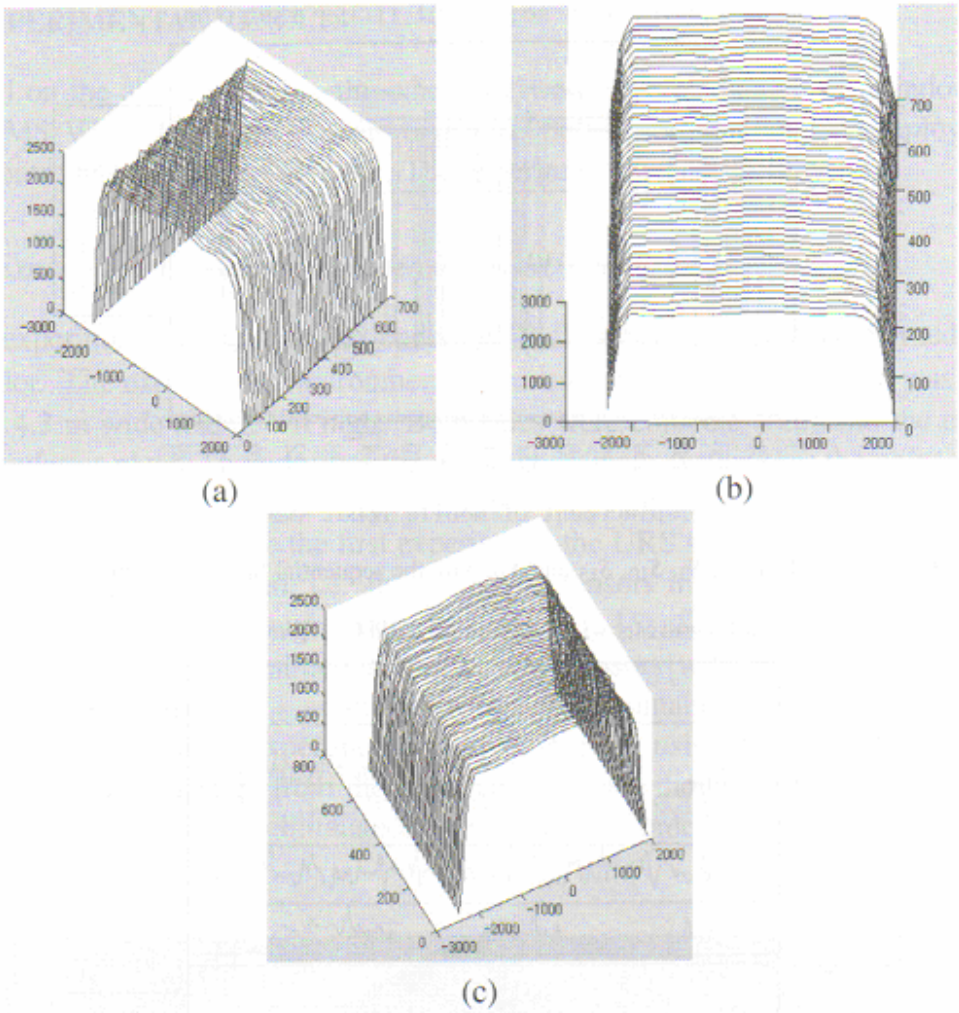

Figure 11. Constructed model of the tunnel. (a) Left side of the corridor. (b) Ceiling of the corridor. (c) Right side of the corridor.

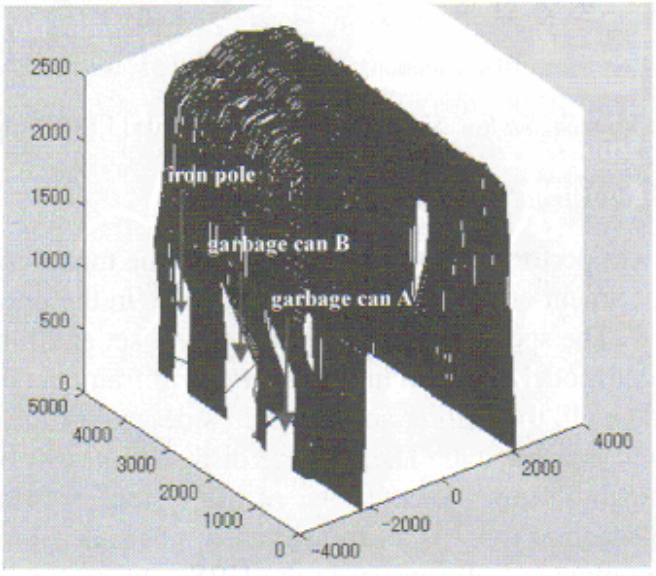

Figure 12. Constructed model of the corridor (5 m).

5 m corridor is given in Fig. 12 as a wireframe, in which the garbage can A, garbage can B and a iron pole in Fig. 8 can be clearly perceived.

5.3. Tunnel inspection experiment results

The experiment was performed in a concrete garage, which we call the pseudo-tunnel. The experiment environment is shown in Fig. 13. The pseudo-tunnel is 5 m long, 3 m wide and 2 m high. First the autonomous mobile robot moved through the pseudo-tunnel and the standard tunnel model T_S is constructed. Then, as a pseudo-deformation of the tunnel inner wall, a box with the volume of $300 \times 220 \times 60$ (mm^3) was pasted to the inner wall of the pseudo-tunnel. The autonomous mobile robot moved through the pseudo-tunnel again and the update pseudo-tunnel model T_U was constructed. Then, the matching between T_S and T_U was performed. The threshold value E_T to binarize the matching error was set at 25 mm and the threshold value N_T to filter the '1'-clumps in the binarized matching error image was set at 3. These values were determined experimentally. The opening of the ultrasonic sensor, α, was set at 12° [6]. The matching between T_S and T_U is shown in Fig. 14. The region surrounded by the white line shows the deformation area detected. The matching error was plotted on xy plane as shown in Fig. 15. The width, length and height of the deformation region were 305, 229 and 64 mm.

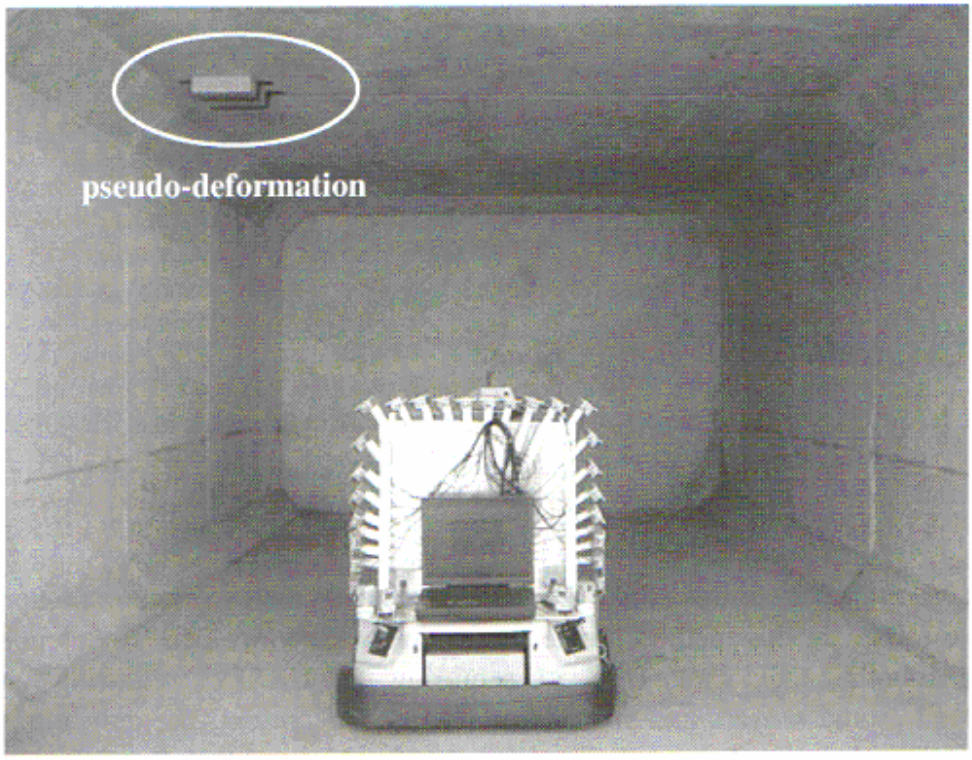

Figure 13. Concrete tunnel inspection experiment scene.

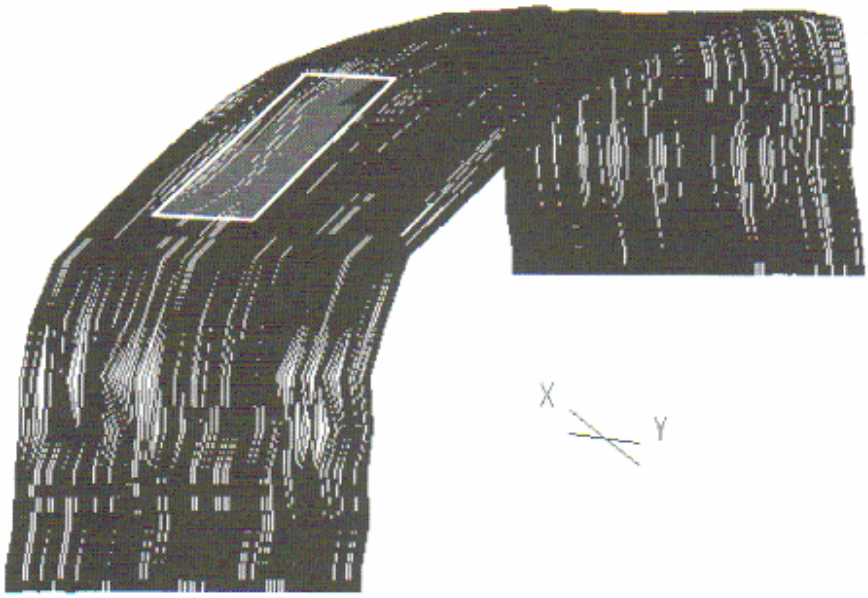

Figure 14. Matching result between T_S and T_U, plotted at a scale of 0.1.

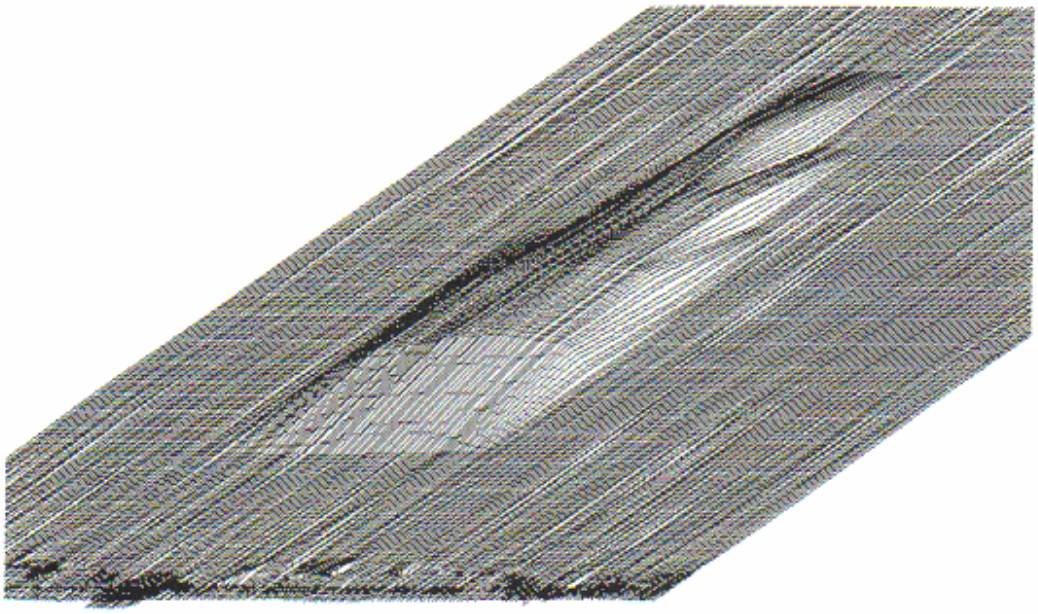

Figure 15. Matching error between T_S and T_U, plotted at a scale of 0.3.

6. CONCLUSIONS

We have proposed an automatic tunnel inspection method using an autonomous mobile robot. In this method, tunnel inspection is performed by an autonomous mobile robot mounted with a URS/VC semi-ring. The URS/VC semi-ring consists of 24 ultrasonic sensors and six video cameras. At present, the only ultrasonic sensors have been implemented. The URS semi-ring is used to detect deformations of the tunnel inner wall, such as 'swell', 'hollow', etc. An important issue comes in

with using multiple URSs, i.e. crosstalk. To solve this problem, we employed the extended EERUF algorithm to fire ultrasonic sensors in the URS semi-ring.

The experiments were performed in a corridor and concrete garage. These experimental environments are very similar to real concrete tunnels. The experimental results show that the URS semi-ring can 'see' the environments (the concrete tunnels) precisely. When the speed of the mobile robot is set at 20 mm/s, the host computer can read the ultrasonic sensors at intervals of 14 mm. That is to say, the inspection division is 14 mm. This value is enough for huge concrete tunnels. If the mobile robot moves at a higher speed, the inspection division will become longer. Because this inspection system also outputs the coordinates of the mobile robot in the world coordinate system, it is able to determine where the deformation exists and how large the deformation is. Thus, the inspection system can make a mark on the ground (e.g. red point), the human inspectors go into the tunnel and find the mark on the ground, and check the specific area of the tunnel inner wall. This greatly reduces the inspection time and saves on the labor.

Using this inspection system, the tunnel is inspected completely and automatically, without any damage to the tunnel inner wall. If multiple inspection robots are employed, starting from different places inside the tunnel, the tunnel can be inspected very efficiently. In addition, the ultrasound waves are harmless to the human body, and thus this inspection robot can cooperate and coexist with people.

At present, only the ultrasonic sensors have been implemented on the URS/VC semi-ring. Future work is to mount the video cameras on the USVC and perform the experiments in the real tunnels.

REFERENCES

1. F. Yao, G. Shao, A. Tamaki, H. Yamada and K. Kato, Development of an automatic concrete tunnel inspection system by an autonomous mobile robot, in: *Proc. IEEE Int. Workshop on Robot–Human Interaction*, Osaka, Japan, pp. 74–79 (2000).
2. J. Borenstein and Y. Koren, Error eliminating rapid ultrasonic firing for mobile robot obstacle avoidance, *IEEE Trans. Robotics Automat.* **11** (1), 132–138 (1995).
3. A. M. Flynn, Combining sonar and infrared sensors for mobile robot, *Int. J. Robot. Res.* **7** (6), 5–14 (1988).
4. T. Ishiyama, T. Takahashi and E. Nakano, The probability of erroneous measurement caused by a crosstalk in multiple sonars, *J. Robotics Soc. Jpn* **17** (4), 526–533 (1999).
5. L. Jetto, S. Longhi and G. Venturini, Development and experimental validation of an adaptive extended Kalman filter for the localization of mobile robots, *IEEE Trans. Robotics Automat.* **15** (2), 219–228 (1999).
6. F. Yao, G. Shao, A. Tamaki, H. Yamada and K. Kato, Development of 3D-ultrasonic-sensor and its application to the construction of large-scale environment model, in: *Proc. 30th Int. Symp. on Robotics*, Tokyo, pp. 305–310 (1999).
7. Polaroid Corp., Ultrasonic Components Group, Cambridge, MA (1989).
8. J. Borenstein and Y. Koren, Obstacle avoidance with ultrasonic sensors, *IEEE Trans. Robotics Automat.* **4** (2), 213–218 (1988).
9. O. Bozma and R. Kuc, Characterizing pulses reflected from rough surface using ultrasound, *J. Accoust. Soc. Am.* **89** (6), 2519–2531 (1991).

10. L. Kleeman and R. Kuc, Mobile robot sonar for target localization and classification, *Int. J. of Robotics Res.* **14** (4), 295–318 (1995).
11. J. Borenstein and Y. Koren, Real–time obstacle avoidance for fast mobile, *IEEE Trans. Syst. Man Cybernet* **19** (5), 1179–1187 (1989).
12. H. P. Moravec, Sensor fusion in certainty grids for mobile robots, *AI Mag.* (Summer), 61–74 (1988).
13. L. Kleeman, Fast and accurate sonar trackers using double pulse coding, in: *Proc. IEEE/RSJ Int. Conf. on Intelligent Robots and Systems*, Kyongju, pp. 1185–1190 (1999).
14. L. Kleeman, Real time mobile robot sonar with interference rejection, *Sensor Rev.* **19** (3), 214–221 (1999).

ABOUT THE AUTHORS

Fenghui Yao received the BE degree from Dalian Maritime University, China, in 1984, and ME and DrEng degrees from Kyushu Institute of Technology, Kitakyushu, in 1988 and 1992, respectively. From 1992 to 1994, he worked at Soliton Systems as a Software Engineer. He worked as a Research Associate in the Faculty of Engineering, Kyushu Institute of Technology, from 1994 to 1996. He joined the University of East Asia, Shimonoseki, in 1997. Currently, he is an Associate Professor at the Graduate School of Integrated Science and Arts, University of East Asia. His current research interests are image processing, intelligent mobile robots, multimedia information processing, computer architecture and parallel processing. He is a member of the IEEE, RSJ, IPSJ, IEICE and BMFSA.

Guifeng Shao received the DrEng degree from Kyushu Institute of Technology in 1995. She is currently an Associate Professor at the Department of Commerce Science, Seinan Gakuin University. Her research interests are natural language understanding, knowledge representation, image processing, mobile robots, and multimedia information processing. She is a member of the IPSJ.

Ryoichi Takaue received the BE degree from Kyushu Institute of Technology, Kitakyushu in 1973, the ME degree from Kumamoto University in 1976 and the DrEng degree form Kyoto University in 1988. He worked as a Research Associate in the Faculty of Engineering, Kyushu Institute of Technology, from 1977 to 1997. He joined the University of East Asia, Shimonoseki, in 1997. Currently, he is an Associate Professor at the Graduate School of Integrated Science and Arts, University of East Asia. His current research interests are photothermal physics, surface and interface analysis, and sensor fusion. He is a member of the JSAP and BMFSA.

Akikazu Tamaki received the BE and ME degrees from Kyushu Institute of Technology, Kitakyushu, in 1969 and 1971, respectively. He worked in the Faculty of Engineering, Kyushu Institute of Technology, Kitakyushu, from 1971 to 2000, as a Lecturer. He joined the University of East Asia, in 2000. Currently, he is an Associate Professor at the Graduate School of Integrated Science and Arts, University of East Asia. His present research interests are computer vision, neural networks and computer music. He is a member of the IEEE, IPSJ, ACM, IEICE and BMFSA.